Response of surface ozone concentration to emission reduction and meteorology during the COVID-19 lockdown in Europe

Adrien Deroubaix[1], Guy Brasseur[1,2], Benjamin Gaubert[2], Inga Labuhn[3], Laurent Menut[4], Guillaume Siour[5], Paolo Tuccella[6]

1. Max Planck Institute for Meteorology, Hamburg, Germany
2. Atmospheric Chemistry Observations & Modeling Laboratory (ACOM), National Center for Atmospheric Research, Boulder, CO, USA
3. University of Bremen, Institute of Geography, Bremen, Germany
4. LMD/IPSL, Ecole Polytechnique, Université Paris Saclay, ENS, IPSL Research University; Sorbonne Université, CNRS, Palaiseau, France
5. Laboratoire Interuniversitaire des Systèmes Atmosphériques (LISA), UMR CNRS 7583, Université Paris Est Créteil et Université de Paris, Institut Pierre Simon Laplace, Créteil, France
6. Departement of Physical and Chemical Sciences, University of L'Aquila, 67010 L'Aquila, Italy

Abstract

The lockdown period (March-May 2020) during the COVID-19 pandemics in Europe led to a reduction in the anthropogenic emissions of primary pollutants. For ¾ of over 1100 available monitoring stations, the average NO_2 concentrations decreased by at least 2.7 $\mu g.m^{-3}$ (or 25%) compared to the average concentrations recorded during the same period of the previous seven years. The O_3 response differed spatially, with positive anomalies in northern Europe and negative anomalies in southwestern Europe. Reduced cloudiness and related enhanced radiation in northern Europe played a significant role in the increase of surface ozone concentrations by shifting the photochemical partitioning between NO_2 and O_3 toward more ozone. The level of total oxidant ($Ox = O_3 + NO_2$) remained unchanged except in southwestern Europe where it decreased. Several episodes lasting a few days of high level of total oxidants were observed in northern Europe. Our results illustrate the complexity of the atmospheric response to the unprecedented reduction in the emission of primary pollutants.

Key Points

- Surface NO_2 concentrations were reduced by at least 2.7 µg.m^{-3} (25% in relation to the same period of the previous seven years) in ¾ of the monitoring stations across Europe during the COVID-19 lockdown period.
- Surface O_3 concentrations were anomalously high in northern Europe, related to low cloudiness and high radiation.
- The level of total oxidant remained unchanged in northern Europe and was reduced in southwestern Europe.

1. Introduction

COVID-19 lockdown restrictions were imposed worldwide in the early months of 2020, first in China starting in January 2020, and starting in early and mid-March across the European continent. In mid-May, restrictions started to be gradually lifted in Europe. Consequently, anthropogenic emissions, especially those related to traffic, were substantially reduced first in China (Le et al., 2020, Shi & Brasseur, 2020) and later elsewhere. Concentration of nitrogen dioxide (NO_2) observed at monitoring stations decreased by up to 60%, whereas a simultaneous increase in ozone (O_3) concentration by a factor 1.5 to 2 was reported (Shi & Brasseur, 2020).

Substantial changes in NO_2 columns measured by the spaceborne TROPOMI instrument have been reported at locations with heavy lockdown measures due to the COVID-19 pandemics. In many Chinese cities, NO_2 column densities decreased by at least 40% (Bauwens et al., 2020). In North American and European cities, a decrease of up to 40% was observed (Bauwens et al., 2020). In Spain, for example, the average reduction of NO_2 during the lockdown compared to a "business-as-usual" emission scenario has been estimated to be close to 40% using machine learning fed by meteorological data (Petetin et al., 2020).

Disentangling the lockdown effects on NO_2 from the natural variability induced by meteorological conditions is essential to build accurate emissions for air quality modeling (Goldberg et al., 2020). Further, short-term perturbations of NO_2 must be put in the context of the long-term trends of pollutant concentrations. Over the two last decades, NO_2 trends have been negative in Europe, while O_3 concentrations remained high (Colette et al., 2015, Yan et al., 2019).

Ordoñez et al. (2020) showed that the ozone concentration increased in Europe during the lockdown, except in the Iberian Peninsula and in the southwestern part of France. Using general additive models at each monitoring station to attribute the changes in the surface O_3 concentrations, they conclude that the meteorological variability outweighed the effects of emission reductions both in urban and in rural areas.

The numerous links between ozone formation and meteorology, involving several processes, raise questions about the meteorological influence on the oxidation capacity of the low troposphere, especially in urban areas where NO_2 reductions were largest (Kroll et al., 2020). Moreover, based on a modelling study, Menut et al. (2020) demonstrated that the ozone perturbation during the lockdown period was different in urban areas throughout Western Europe due to non-linear chemical effects. This is further highlighted by Sicard et al. (2020) showing a variable ozone increase in four southern European cities (Nice in France, Rome in Italy, Valencia in Spain and Turin in Italy), ranging from 2.4% in Valencia to 27% in Turin compared to 2017-2019. The purpose of the present study is to understand the causes of the surface ozone concentration change in response to the exceptional short-term reduction of anthropogenic emissions during the COVID-19 lockdown period in Europe. We characterize anomalies in the concentrations of five regulated pollutants (CO, NO_2, SO_2, O_3 and PM_{10}) in rural and urban environments (compared to the previous seven years) associated with anomalies of different meteorological variables. This allows us to investigate possible causes of the observed ozone concentration changes, which could be related to the changes in primary pollutant emissions, but

also to concomitant changes in meteorology and photochemistry. We will further focus on the evolution of the total oxidant concentrations (also called odd oxygen), *i.e.* Ox ≈ O_3 + NO_2 (Wang and Jacob, 1998).

Our study is based on measurements made at surface monitoring stations together with modeled meteorological conditions. Air quality data and other data sources are referred to in Section 2. Section 3 presents the distribution of the concentration changes and Section 4 their spatial patterns. The ozone response is analyzed in Section 5, and its consequences on the total oxidant level in Section 6. A discussion and perspectives are given in Section 7.

2. Data and methods

Air quality, meteorological conditions and population density data were obtained for the spatial domain under consideration that extends from 11°W to 19°E and from 35°N to 60°N. We focus on the period 18 March - 18 May of years 2013 to 2020.

Measured concentrations of regulated pollutants from national monitoring networks were retrieved from the European Air Quality e-Reporting database (*hereafter* AirBase), which provides near-real time air quality data for Europe in a standardized format (AQ e-Reporting, 2020). The data available are hourly concentrations in the case of CO, NO_2, SO_2, and O_3, and daily concentrations in the case of PM_{10}. The domain includes 1680 AirBase stations. However, data from 1308 stations were used in this study as we selected only with at least 70% of days of the period 18 March - 18 May (for each year) filled with at least one hourly value for the respective pollutant.

Meteorological variables were obtained from the European Centre for Medium-Range Weather Forecasts - Integrated Forecasting System (ECMWF-IFS) at a spatial resolution of 0.125° x 0.125°. Through the Copernicus Atmosphere Monitoring Service (CAMS) near-real-time output, 6-hour analyses of the following meteorological variables were downloaded (Inness et al., 2019): 2m-temperature, 2m-dew point, mean sea level pressure, potential vorticity at 300 hPa, 10m-zonal wind, 10m-meridional wind, total cloud cover, and downward surface solar radiation (forecast accumulated over 24 hours). The 2m-relative humidity field was calculated on the basis of the temperature and dew point fields. The 10m-wind speed field was calculated from the zonal and meridional wind fields. The potential vorticity at 300 hPa is selected as a proxy for the downward stratospheric transport (*e.g.* Doche et al., 2020).

Population density data were taken from the Gridded Population of the World Version 3 (GPWv3) data set, which has a spatial resolution of 1 km x 1 km (CIESIN/CIAT 2005; presented over the studied domain in Fig. S1). We define “urban” and “rural” station types based on the European Union “high-density areas” threshold of 1500 inhabitants per km². This leads to 485 “urban” stations (above this threshold) and 1195 “rural” stations (below this threshold). With this methodology, “urban” sites are clearly located in areas with high anthropogenic emissions, whereas “rural” sites include a large diversity of environments.

We analyze temporal anomalies by comparing the atmospheric quantities for the period 18 March 2020 - 18 May 2020 (*i.e.* the lockdown period) with the same quantities for the previous seven years (2013-2019). For pollutants, we use two metrics to characterize the chemical environment at each station location using hourly measurements: (a) the mean concentrations; and (b) the median of the hourly daily maximum concentrations. Anomalies are expressed as absolute and relative differences between 2020 and the 2013-2019 average.

3. Changes in the concentrations of regulated pollutants

At each station, we compare the mean concentrations of regulated pollutants during the lockdown period with the mean concentrations of the same pollutants averaged over the previous seven years. The distribution of absolute and relative differences (*i.e.* anomalies) given by five percentiles (10, 25, 50, 75, 90) are presented for all stations (Tab. 1) and with a distinction between “urban” and “rural” stations (Tab. S1 and S2).

We note a clear reduction in the average concentrations of NO_2, for which even the percentile 90 of the anomalies is negative (Tab. 1). Thus, at least 90% of the stations (P10) have monitored a reduction in the NO_2 concentrations of at least 1 $\mu g.m^{-3}$ or 14%. In the case of O_3, the median (P50) of the anomalies is positive (4.3 $\mu g.m^{-3}$ or 7%), which means that a majority of the available stations have reported an increase in the average concentration. For PM_{10}, the median (percentile 50) of the anomalies is slightly negative (-0.7 $\mu g.m^{-3}$ or -4%), and the percentile 75 (P75) is positive (1.6 $\mu g.m^{-3}$ or -6%). It is worth noticing that on 28 March, a severe dust event occurring over southeast Europe led to strong positive PM_{10} anomalies for three days (Menut et al., 2020).

Our confidence in the database to represent accurately the distribution of the concentration anomalies across Europe is high for NO_2 and O_3 because 71% and 68% of the stations provide data (*i.e.* 1196 and 1148 stations respectively), and to a lesser extent for PM_{10} with 53% (*i.e.* 895 stations). For CO and SO_2, the number of available stations reporting data is low (12% and 27%). Nevertheless, we observe that the median of the anomalies is -8.8 $\mu g.m^{-3}$ (-4%) for CO and -0.2 $\mu g.m^{-3}$ (-11%) for SO_2.

***Table 1**. Anomalies of the mean concentrations of CO, NO_2, SO_2, O_3 and PM_{10} in 2020 compared to the average of the previous seven years (2013-2019) for the period 18 March to 18 May, measured at 1308 AirBase stations. The distribution of the anomalies for all stations is given by five percentiles (P10, P25, P50, P75, P90); "% avail." indicates the percentage of available stations. Upper part of the table: anomalies in terms of concentrations (in µg.m^{-3}); lower part of the table: relative change (in %) against the 7-year average.*

µg.m^3	P10	P25	P50	P75	P90	% avail.
CO	-85.3	-42.5	-8.8	64.8	214.6	*12*
PM_{10}	-4.2	-2.6	-0.7	1.0	3.0	*53*
NO_2	-12.1	-8.5	-5.2	-2.7	-1.0	*71*
O_3	-9.7	-2.6	4.3	8.5	11.7	*68*
SO_2	-1.9	-0.9	-0.2	0.2	1.1	*27*

%	P10	P25	P50	P75	P90	% avail.
CO	-30	-16	-4	23	82	12
PM_{10}	-22	-14	-4	6	16	53
NO_2	-59	-50	-37	-25	-14	71
O_3	-13	-4	7	14	20	68
SO_2	-55	-35	-11	15	60	27

One can expect the strongest reduction in concentrations of primary pollutants to happen in areas where human activities are the most intense. In other words, the reduction may be stronger at "urban" stations than at "rural" stations. To test this hypothesis, the same analysis is performed separately for "urban" and "rural" stations (as defined in Sect. 2) to investigate the pollutant concentration changes depending on population density.

Our analysis reveals that the relative concentration changes are very similar for "urban" and "rural" stations (Tab. S1 and S2). As expected, the NO_2 absolute anomalies are highest for "urban" stations (-7.9 µg.m^{-3}) compared to "rural" stations (-3.9 µg.m^{-3}), but the relative changes are similar for both types of stations (-40% for "urban" and -35% for "rural" stations). This result suggests that the mobility restrictions have led to comparable relative reductions of NO_2 emissions in urban and rural areas.

The O_3 absolute anomalies show an increase for both "urban" (6.8 µg.m^{-3}) and "rural" stations (3.1 µg.m^{-3}), although the relative anomalies show comparable increase for those two areas (+11% in "urban" station and +5% in "rural" stations). This result clearly suggests that areas with stronger reduction in NO_2 concentrations led to higher increase in O_3 concentrations. We conclude that a clear reduction of the NO_2 concentration averages was monitored during the lockdown period but this is not the case for O_3 and PM_{10} concentrations.

4. Spatial patterns of nitrogen dioxide and ozone

Although our analysis show that there are distinct pictures for NO_2 and O_3 concentrations during the lockdown period, we investigated if there were spatial discrepancies for NO_2, O_3 and PM_{10} anomalies calculated over the period 18 March to 18 May. Following the same methodology, we present the absolute and relative differences between 2020 and the previous seven years on a single figure, displaying the information on maps where each station is colored depending on absolute differences and sized based on the relative differences.

The NO_2 anomalies depict a clear reduction in mean concentrations (mostly greater than 30%) during the lockdown all over Europe (Fig. 1a). The strongest changes occur in southern Europe (Spain, France, Italy) where the COVID-19 incidence has been among the highest (COVID-19.who.int), and where the strongest mobility restrictions were imposed. Anomalies of daily maximum concentrations show the same spatial pattern (Fig. S2a).

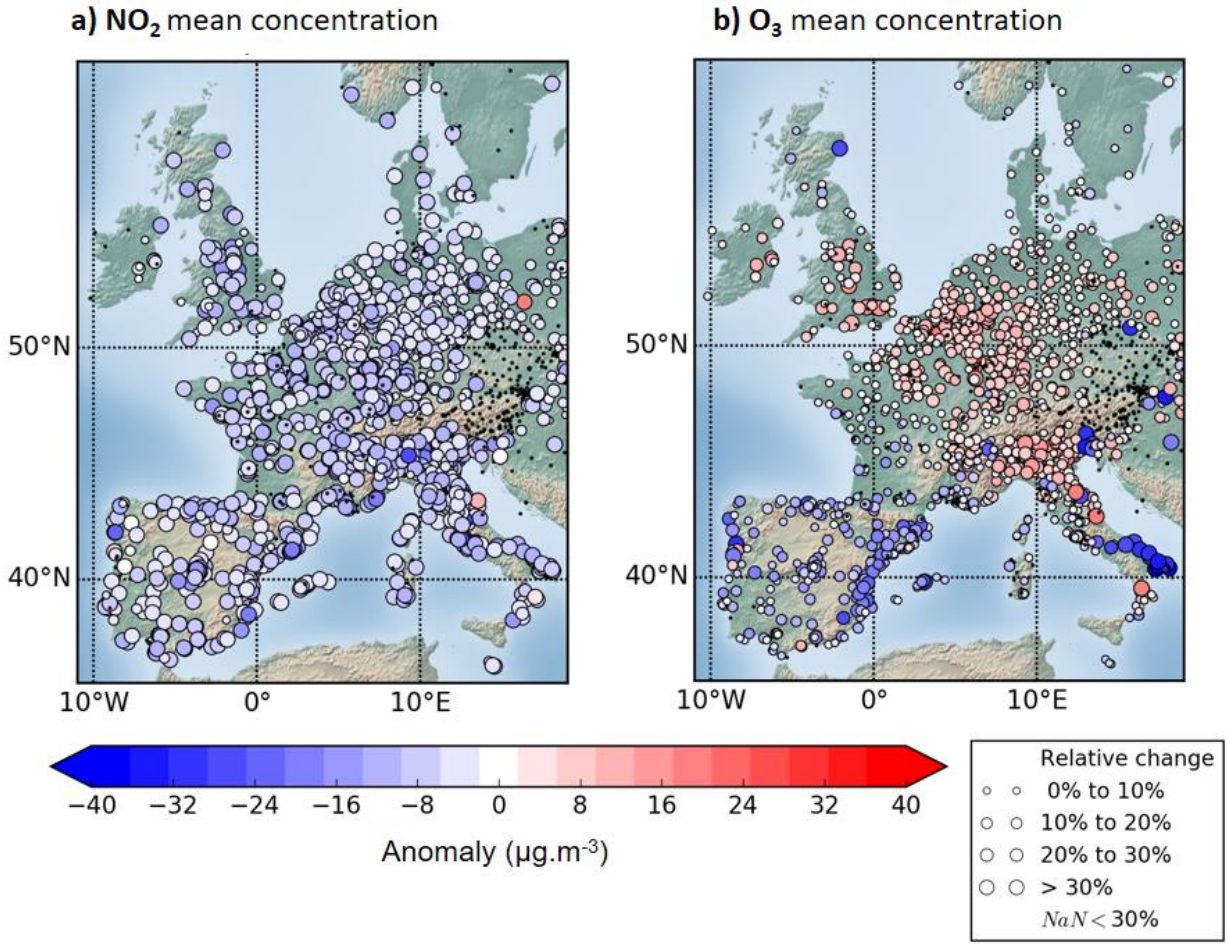

***Figure 1**. Anomalies of **(a)** NO_2 mean concentration and **(b)** O_3 mean concentration at AirBase stations in 2020 compared to the previous seven years (2013-2019) for the period 18 March to 18 May. The dots are colored according to the anomalies in concentration (in µg.m^{-3}) and sized proportionally to the relative change (in %). The black dots correspond to stations with less than 30% of available data.*

Although the negative anomalies in NO_2 concentration occurred everywhere in Europe, we clearly observe regional patterns in O_3, with positive anomalies in the Benelux and negative anomalies in Spain, Portugal and southwestern France (Fig. 1b). In the north of the continent, most of the stations reported positive anomalies in the mean concentrations (ranging from 0% to 30%), whereas in the southwestern part of Europe, negative anomalies were reported (ranging from 0% to -30%). In the region of the French and Italian Alps, the anomalies of O_3 were especially variable (greater than 30% and lower than -30%). As for NO_2, anomalies in median of O_3 daily maximum concentrations are characterized by the same spatial patterns as found in the anomalies of the mean concentrations (Fig. S2b).

We checked if the spatial patterns of PM_{10} anomalies could be related to the patterns of NO_2 and O_3. We found negative PM_{10} anomalies of the mean and of the median of daily maximum concentrations in northern Europe and southwestern Europe (Fig. S3). In Italy and in the Benelux,

there was no spatially consistent pattern in PM_{10} anomalies. Thus, PM_{10} anomalies do not match the ones of NO_2 and O_3.

Our investigations are consistent with Ordoñez et al. (2020) in terms of spatial patterns and quantification of the O_3 anomalies, although they use a different methodology, reference period and definition of the lockdown duration. The contrast in O_3 anomalies between the north and the southwest of Europe does not correspond to the spatial patterns in the PM_{10} anomalies nor to the level of urbanization. Therefore, further analysis on the O_3 response is necessary, which we present in the next section.

5. Ozone response analysis

A comprehensive analysis of the ozone response to the emission reduction of air pollutants during the COVID-19 lockdown must consider the different potential drivers of ozone changes. These include the emissions of precursor species such as NO_x, CO and volatile organic carbon (VOC), as well as surface dry deposition, together with the meteorological situation (atmospheric humidity and temperature, cloudiness and solar irradiance, precipitation, wind direction and speed, and intrusion of stratospheric air masses; *e.g.* Monks et al., 2015). The analysis must also distinguish between regional (background) and local (urban) contributions.

The spatial patterns of O_3 anomalies in Europe could be interpreted as a modification in the partitioning between O_3 and NO_2 or as a shift in chemical regimes (*i.e.* a change in the NO_x/VOC ratio), which both result from a reduction in the primary anthropogenic emissions during the lockdown period. At the same time, changes in regional ozone could be related to meteorological disturbances. The contribution of each process could not be quantified with the available data sets, but some evidence for the relative importance of their influence can be obtained. We use three indicators: (i) meteorological variables, (ii) the distinction between “urban” and “rural” stations, and (iii) the relationship with NO_2 anomalies.

During the lockdown period, the meteorology in northern Europe, especially in the Benelux region, was characterized by anomalously low humidity (Fig. S4b and S4c), high pressure (Fig. S4d), low cloudiness (Fig. 2a), low wind speed (Fig. S4f, S4g and S4h), high surface solar radiation (Fig. S4i), and downward transport of air from the stratosphere (Fig. S4e). A positive anomaly in the 2m-temperature was observed in France, south of the dry anomaly region (Fig. S4a). In southern Europe, specifically in Spain, where ozone concentrations were anomalously low, total cloud cover and relative humidity were particularly high, associated with low solar radiation and temperature compared to the previous seven years.

The spatial patterns of several meteorological anomalies seem to match the O_3 anomalies. We analyze therefore the correlation coefficients of the anomalies in the ozone concentrations against the anomalies of ten meteorological variables at each site (*i.e.* the corresponding grid cell). Correlation coefficients are calculated for all monitoring stations, as well as for “urban” and “rural” stations separately (Tab. 2).

Table 2. *Correlation coefficients between O_3 mean concentration anomalies and anomalies in (1) 2m-temperature, (2) 2m-dew point, (3) 2m-relative humidity, (4) mean sea level pressure, (5) potential vorticity at 300 hPa, (6) 10m-zonal wind speed, (7) 10m-meridional wind speed, (8) 10m-wind speed, (9) total cloud cover, and (10) downward surface solar radiation. Anomalies are calculated for 2020 compared to the previous seven years (2013-2019) for the period 18 March to 18 May. The distinction between "urban" and "rural" sites is defined by a population density threshold of 1500 inhabitants/km². In bold font, correlation coefficients greater than 0.5 or lower than -0.5.*

Correlation coeffcient (R)	Mean O3 anomalies		
	All	Urban	Rural
2m-T ano.	0.20	0.14	0.18
2m-Dew point ano.	-0.42	-0.46	-0.43
2m-RH ano.	**-0.54**	**-0.56**	**-0.54**
Pot. Vort. 300hPa ano.	0.43	0.47	0.44
MSL press. ano.	-0.35	-0.37	-0.33
10m-Zonal wind ano.	-0.15	-0.19	-0.09
10m-Merid. wind ano.	-0.33	-0.42	-0.28
10m-Wind speed ano.	0.25	0.24	0.26
Tot. cloud cov. ano.	**-0.61**	**-0.58**	**-0.61**
Surf. solar rad. down. ano.	**0.59**	**0.58**	**0.60**

The signs of these correlation coefficients (*i.e.* R) are consistent with the interpretation that specific meteorological conditions (less clouds, higher radiation, lower humidity, higher pressure) lead to an increase in the ozone concentration. The spatial variability of the ozone anomalies explained with meteorological variable anomalies (*i.e.* R^2) are highest for the total cloud cover (R^2 = 0.36), the downward surface solar radiation (R^2 =0.35), and the 2m-relative humidity (R^2 = 0.30). Thus, the spatial variability of these meteorological anomalies is highly related with the spatial variability of ozone anomalies (*i.e.* R^2 ranges from 0.30 to 0.36).

The correlation coefficients between the O_3 anomalies against meteorological anomalies are similar for "urban" and "rural" sites (Tab. 2), which suggests that the anomalies in the ozone concentration are linked with the anomalies in the cloudiness (or radiation) across Europe during the lockdown period. Figure 2b shows that the O_3 anomalies follow the same linear relationship with the total cloud cover anomalies for urban as for other environments, which supports the interpretation of a regional scale influence of cloudiness (and therefore solar radiation) on ozone anomalies.

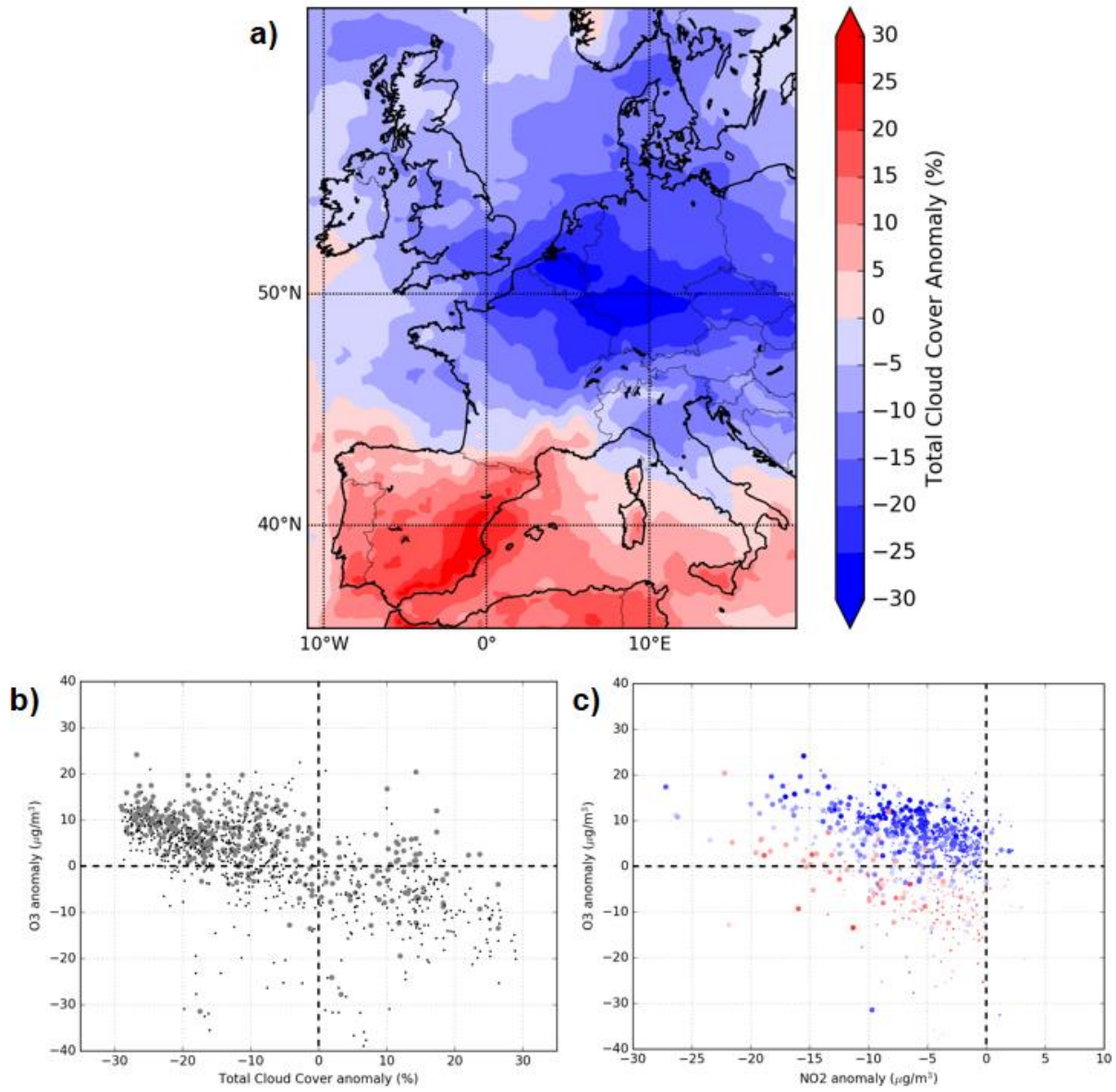

***Figure 2**. **(a)** Total cloud cover anomalies from the ECMWF-IFS model data at 0.125°x0.125° resolution. Anomalies of the mean values in 2020 compared to the previous seven years (2013-2019) for the period 18 March to 18 May. **(b)** O_3 anomalies against total cloud cover anomalies at AirBase stations. **(c)** O_3 anomalies against NO_2 anomalies at AirBase stations. Large dots in (b) and (c) represent "urban" stations and small dots represent "rural" stations. "Urban" stations are defined by a population density threshold of 1500 inhabitants/km². Dots in (c) are colored depending on total cloud cover anomalies of panel (a) at each station.*

We account for the cloudiness in the O_3 against NO_2 scatterplot by coloring the dots as a function of the anomalies in the total cloud cover (Fig. 2c). The NO_2 anomalies are to be inversely proportional to the O_3 anomalies at "urban" stations. The total cloud cover anomalies add another layer of variability on top on this relationship, because the distribution of the blue and red dots in

the scatterplot follows two parallel lines. This result could be due to either a modification in the partitioning between O_3 and NO_2 or a shift in chemical regimes, which both need solar radiation to be efficient.

Radiation and clouds have played a major role in ozone's response to emission reductions. In addition, but to a lesser extent, the advection and subsidence of air masses (with a different level of ozone concentration) could have contributed. Since the correlations between all meteorological variables are high, and non-linear effects on ozone are expected, we only conclude that cloudiness (and radiation) anomalies have contributed to the north-southwest contrast observed in the ozone concentration anomalies in Europe during the COVID-19 lockdown.

6. Level of total oxidant

In order to understand the specificity of the ozone response during the lockdown, we investigate the spatial and temporal variability of daily mean total oxidant concentrations (*i.e.* $Ox \approx O_3 + NO_2$). We first investigate the spatial patterns of Ox anomalies at the regional scale (Sect. 6.1), and we focus then on urban environments, analyzing the anomalies in day-to-day variability and in averaged diurnal cycles of NO_2, O_3 and Ox concentrations (Sect. 6.2).

6.1 At the regional scale

Many processes can be invoked to explain the anomalies in surface total oxidant concentrations: (i) transport and deposition, and (ii) local photochemical production (thus related to the primary emissions of nitrogen and organic carbon), and (iii) loss by oxidation of other atmospheric species (Jacob, 1999). However, a modification in the partitioning between O_3 and NO_2 does not modify the level of total oxidant. The increase in ozone concentrations coinciding with a NO_2 decrease is a consequence of the daytime photo-stationary state of ozone (Leighton, 1961) in which the reaction of ozone with NO (producing NO_2) is compensated by the photolysis of NO_2 (producing ozone).

Figure 3 presents a map of the mean Ox concentration anomalies in Europe compared to the previous seven years. In the rural areas in northern Europe (where $NO_2 << O_3$), the Ox anomalies are generally positive but low (less than 20%). The situation is different in southern Europe. In southwestern Europe, the Ox anomalies are strongly negative, reaching -30% at several stations. In Italy, they are more variable with values ranging from -20% to +20%. In all urban areas (where $NO_2 \approx O_3$), the anomalies seem to be of the same order of magnitude as in the surrounding rural areas.

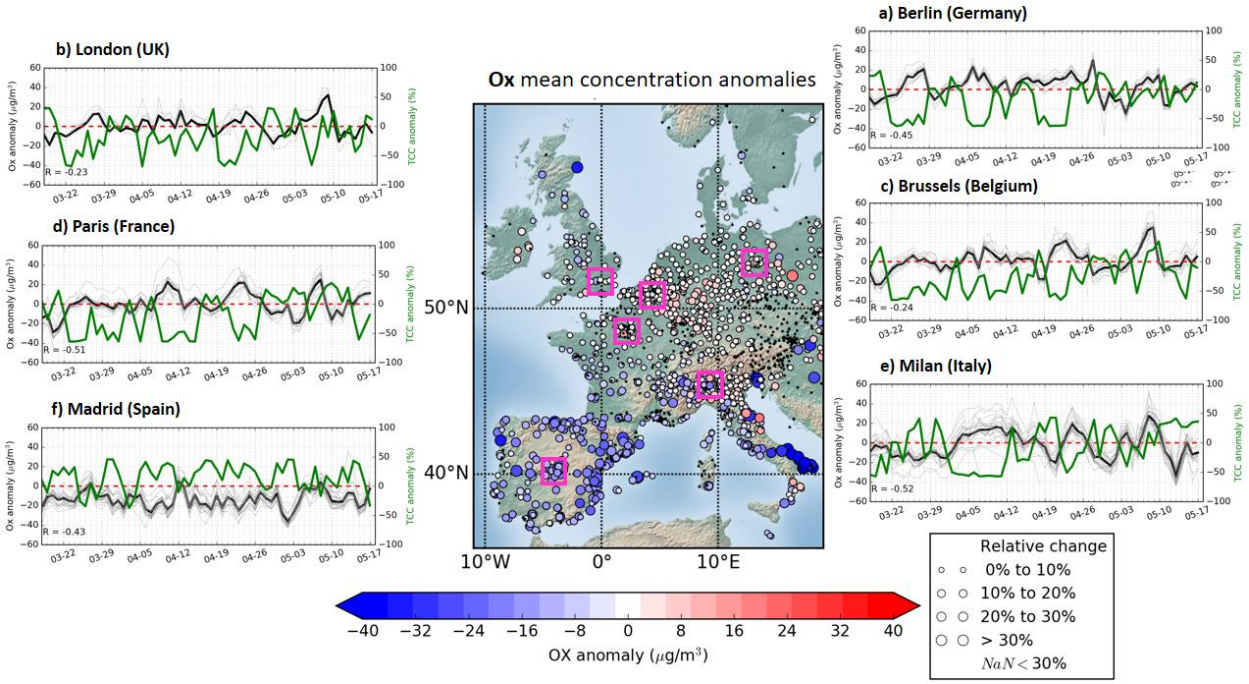

***Figure 3**. Map of mean total oxidant (Ox) concentration anomalies at AirBase stations in 2020 compared to the previous seven years (2013-2019) for the period 18 March to 18 May. The dots are colored according to the anomalies in concentration (in µg.m^{-3}) and sized proportionally to the relative change (in %). The black dots correspond to stations with less than 30% of available data. The violet squares correspond to the location of the six major European cities for which we present the daily total clover cloud anomalies (green line) and daily Ox mean concentration anomalies compared to the average of previous seven years at each station (grey lines) and for the average of all stations (black line) in (a) Berlin (Germany), (b) London (UK), (c) Brussels (Belgium), (d) Paris (France), (e) Milan (Italy) and (f) Madrid (Spain).*

6.2 In urban environments

We select six major cities located in contrasted regions of the O_3 anomaly pattern (see Fig. 1): Berlin (Germany), London (UK), Brussels (Belgium), Paris (France), Milan (Italy) and Madrid (Spain). We collect the data from all monitoring stations within +/- 0.5° of the center of these cities (that we define as 13.4°E/52.5°N, 0.1°W/51.5°N, 4.3°E/50.8°N, 2.3°E/48.9°N, 9.2°E/45.4°N, 3.7°W/40.4°N respectively).

Day-to-day variability and diurnal cycle anomalies are calculated for NO_2, O_3 and Ox concentrations as differences with the average of the previous seven years (Fig. 3, S5 and 4). Anomalies are analyzed based on 13 stations in Berlin, 8 in London, 26 in Brussels, 31 in Paris, 28 in Milan and 27 in Madrid. In each city, the variability between the individual stations is coherent, so that, in the following, we focus on the city average concentration values (Fig. 3, S5 and 4).

When examining the temporal variability of Ox in the six cities under consideration (Fig. 3), we note that the anomalies compared to previous years are small (typically ranging from -20 to +10 $\mu g.m^{-3}$). Madrid represents an exception with larger negative anomalies (ranging from -30 to 0 $\mu g.m^{-3}$). The periods of negative cloud cover anomaly match well the periods of positive O_3 anomaly. The daily total cloud cover anomalies are negatively correlated with the Ox anomalies, with the correlation coefficients ranging from -0.23 to -0.52.

In the major cities of northern Europe (*i.e.* Berlin, London, Brussels and Paris), NO_2 concentrations decreased and O_3 increased during the COVID-19 lockdown period (Fig. S5). We note that the NO_2 decrease was higher in Paris and in Brussels, where lockdown restrictions were stricter than in London and Berlin. In London, the lockdown effect on NO_2 concentrations was clearly visible after mid-April. In Milan, the NO_2 reduction was associated with a high day-to-day variability of the O_3 concentration during the entire period. Compared to the five other cities, Madrid is remarkable because for both NO_2 and O_3 the anomalies are negative.

Several relatively long periods of more than five consecutive days with negative cloud cover anomalies were observed in all cities except Madrid. During these periods, Ox concentrations remained relatively constant and the observed increase in O_3 concentration was compensated by the decrease in NO_2 concentration. However, the correlation coefficients between the anomalies in cloud cover and Ox concentration are variable in the six cities, ranging from -0.06 to -0.42. This is due to the occurrence of some specific events for which, large increases in Ox reaching +20 $\mu g.m^{-3}$ were observed during one or two days. Half of these events were associated with negative cloud anomalies, but the other half were not. Other processes must therefore be invoked such as transport of polluted air masses.

The study of the anomalies in the diurnal cycles of NO_2, O_3 and Ox concentrations provides useful information to confirm our interpretation of the evolution of the level of total oxidant (Fig. 4). We note that NO_2 anomalies remained negative throughout the day and night in all six cities. Except in Madrid, the O_3 anomalies remained positive throughout the day. In Berlin, total oxidant anomalies were positive throughout the day and night, ranging between 1 and 5 $\mu g.m^{-3}$. In London, Brussels and Paris, the total oxidant level decreased overnight (about -5 $\mu g.m^{-3}$) and increased during the day (about +5 $\mu g.m^{-3}$) compared to the average observed over the previous seven years. In Milan, anomalies were (mostly) negative throughout the day and night, ranging between -10 and 1 $\mu g.m^{-3}$. In Madrid, during the day and at night, the level of total oxidant clearly decreased by more than 10 $\mu g.m^{-3}$.

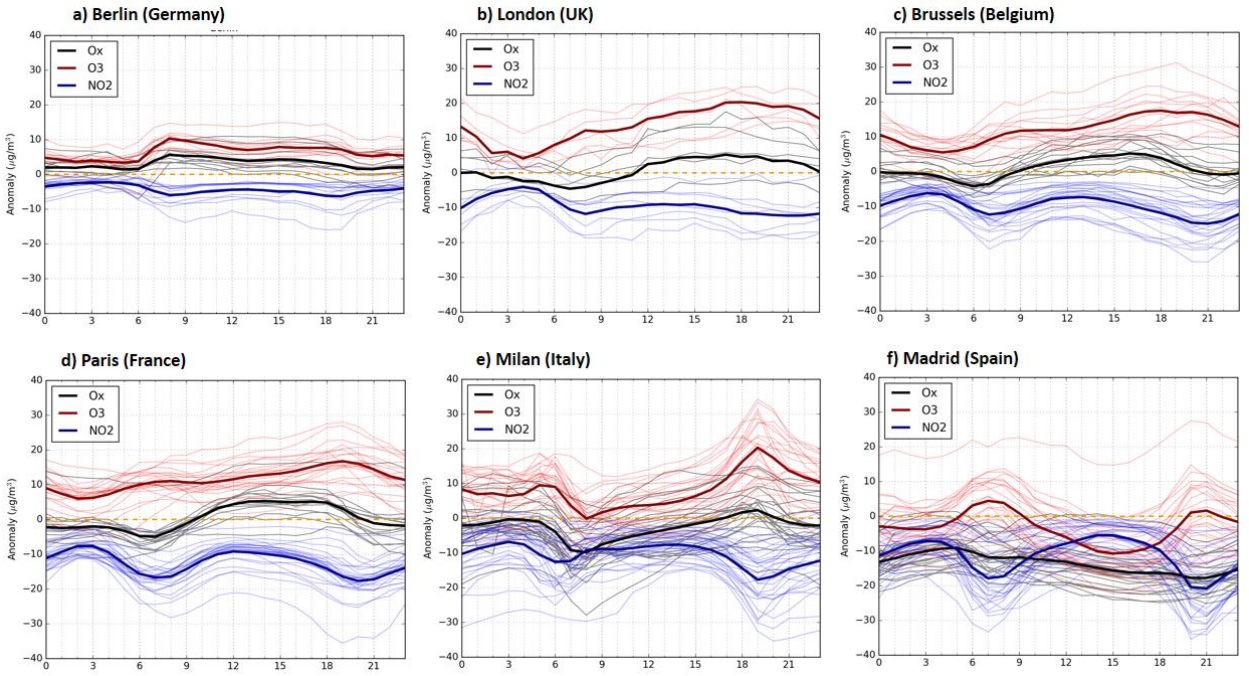

Figure 4. *Hourly mean concentration anomalies of NO_2 (blue lines) and O_3 (red lines) in 2020 compared to the previous seven years (2013-2019) for the period 18 March to 18 May of each monitoring station and of the average of all stations (bold lines) at six major European cities: (a) Berlin (Germany), (b) London (UK), (c) Brussels (Belgium), (d) Paris (France), (e) Milan (Italy) and (f) Madrid (Spain).*

In conclusion, the concentration of total oxidant decreased during the pandemics in southwestern Europe, but remained similar to previous (unperturbed) years in northern Europe. It appears that the observed ozone increase in northern Europe was due primarily to a change in the partitioning between O_3 and NO_2 as driven by positive solar radiation anomalies associated with reduced cloud cover. In addition, several episodes of positive Ox anomalies were noted during a few days, which could be linked to enhanced formation or reduced destruction of ozone, or to the transport of polluted air masses.

7. Summary and perspectives

Our analysis confirms that the COVID-19 lockdown period in Europe has been exceptional in terms of (primary) pollutant concentration change, especially in the case of NO_2 whose concentration decrease was at least 14% for 90% of the monitoring stations relative to the previous seven years. The O_3 concentration response is contrasted between the northern and the southwestern parts of Europe with positive and negative anomalies, respectively. Reduced cloud cover in northern Europe coincided with the positive O_3 anomalies, associated with a low increase of the level of total oxidant. Enhanced cloud cover in southwestern Europe coincided with the negative O_3 anomalies associated with an important decrease of the level of total oxidant.

Radiation and clouds played a major role in ozone's response to emission reductions. Air mass dynamics may have played a lesser role in the increase in ozone (by advection or subsidence).

Episodes of high total oxidant level were observed in northern Europe but an assessment of the role of VOCs is necessary to quantitatively analyze changes in the chemical regime. Despite the lack of concordance of the anomalies of PM_{10} and Ox, we cannot exclude that aerosols have played an important role in the ozone's response through the oxidation VOCs, through the production of inorganic aerosols, or through heterogeneous reactions affecting, for example peroxy radicals (HO_2, RO_2), formaldehyde (HCHO), nitrogen oxides or ozone. Chemistry-transport models can provide these answers. Studies based on observations are essential to refine our estimates and to validate model outputs.

Our results confirm the significant increase in surface concentrations of ozone observed in most parts of Europe during the lockdown period and reported by Venter et al. (2020) and Ordoñez et al. (2020). Ordoñez et al. (2020) attributed this increase primarily to the influence of meteorological parameters rather than to the reduction in the emissions of primary pollutants. In this study, we conclude that the observed increase in ozone was due primarily to a change in the photochemical partitioning between NO_2 and O_3 due to an anomalously low cloud cover, while the level of total oxidant remained unchanged, except in the Iberian Peninsula and in the southwestern part of France, where it decreased.

Understanding the behavior of ozone during the COVID-19 lockdown provides an opportunity to design future pollutant reduction regulations with the purpose of reaching the levels of NO_2 observed during the lockdown. Nevertheless this study illustrates the complexity of the processes affecting ozone in the troposphere and hence the difficulty of implementing efficient regulations targeting air quality impacts.

Acknowledgments

The authors thank Gabriele Pfister, Antonio Caltabiano and Tao Wang for their valuable comments on the manuscript. The National Center for Atmospheric Research is sponsored by the National Science Foundation. The authors are grateful to the EEA (European Environmental Agency) for maintaining and providing the surface concentrations of criteria pollutants over Europe.

All data used in this study are publicly available at the following repository:

Regulated pollutant concentration measurements "Air Quality e-Reporting" at https://www.eea.europa.eu/data-and-maps/data/aqereporting-8 (permanent link: b21a537e763e4ad9ac8ccffe987d6f77)

Meteorological variables "ECMWF CAMS" at https://apps.ecmwf.int/datasets/data/cams-nrealtime

Population density "CIESIN/CIAT 2005 Center for International Earth Science Information Network" at https://doi.org/10.7927/H42B8VZZ

This study is dedicated to Andreas Hilboll from the University of Bremen who passed away during the COVID-19 pandemics.

References

Air Quality e-Reporting (AQ e-Reporting) (2020). Available at https://www.eea.europa.eu/data-and-maps/data/aqereporting-8 (permanent link: b21a537e763e4ad9ac8ccffe987d6f77). Accessed: 2020-07-22.

Bauwens, M., Compernolle, S., Stavrakou, T., Müller, J. - F., Gent, J., Eskes, H., Levelt, P. F., A, R., Veefkind, J. P., Vlietinck, J., Yu, H. and Zehner, C.: Impact of coronavirus outbreak on NO 2 pollution assessed using TROPOMI and OMI observations, Geophys. Res. Lett., (2), 0–3, doi:10.1029/2020GL087978, 2020.Chen, H., Huo, J., Fu, Q., Duan, Y., Xiao, H. and Chen, J.: Impact of quarantine measures on chemical compositions of PM2.5 during the COVID-19 epidemic in Shanghai, China, Sci. Total Environ., 743, 140758, doi:10.1016/j.scitotenv.2020.140758, 2020.

CIESIN/CIAT 2005 Center for International Earth Science Information Network - CIESIN - Columbia University, United Nations Food and Agriculture Programme - FAO, and Centro Internacional de Agricultura Tropical - CIAT. 2005. Gridded Population of the World, Version 3 (GPWv3): Population Count Grid, Future Estimates. Palisades, NY: NASA Socioeconomic Data and Applications Center (SEDAC). doi:10.7927/H42B8VZZ. Accessed 11/2011

Colette, A., Andersson, C., Baklanov, A., Bessagnet, B., Brandt, J., Christensen, J. H., Doherty, R., Engardt, M., Geels, C., Giannakopoulos, C., Hedegaard, G. B., Katragkou, E., Langner, J., Lei, H., Manders, A., Melas, D., Meleux, F., Rouïl, L., Sofiev, M., Soares, J., Stevenson, D. S., Tombrou-Tzella, M., Varotsos, K. V. and Young, P.: Is the ozone climate penalty robust in Europe?, Environ. Res. Lett., 10(8), 084015, doi:10.1088/1748-9326/10/8/084015, 2015.

Doche, C., Dufour, G., Foret, G., Eremenko, M., Cuesta, J., Beekmann, M. and Kalabokas, P.: Summertime tropospheric-ozone variability over the mediterranean basin observed with IASI, Atmos. Chem. Phys., 14(19), 10589–10600, doi:10.5194/acp-14-10589-2014, 2014.

Goldberg, D. L., Anenberg, S. C., Griffin, D., McLinden, C. A., Lu, Z. and Streets, D. G.: Disentangling the Impact of the COVID-19 Lockdowns on Urban NO2 From Natural Variability, Geophys. Res. Lett., 47(17), 0–3, doi:10.1029/2020GL089269, 2020.

Inness, A., Ades, M., Agustí-Panareda, A., Barré, J., Benedictow, A., Blechschmidt, A.-M., Dominguez, J. J., Engelen, R., Eskes, H., Flemming, J., Huijnen, V., Jones, L., Kipling, Z.,

Massart, S., Parrington, M., Peuch, V.-H., Razinger, M., Remy, S., Schulz, M. and Suttie, M.: The CAMS reanalysis of atmospheric composition, Atmos. Chem. Phys., 19(6), 3515–3556, doi:10.5194/acp-19-3515-2019, 2019.

Jacob, D. J. (1999) *Introduction to Atmospheric Chemistry*, Princeton University press. Princeton, NJ.

Kroll, J. H., Heald, C. L., Cappa, C. D., Farmer, D. K., Fry, J. L., Murphy, J. G. and Steiner, A. L.: The complex chemical effects of COVID-19 shutdowns on air quality, Nat. Chem., 12(9), 777–779, doi:10.1038/s41557-020-0535-z, 2020.

Le, T., Wang, Y., Liu, L., Yang, J., Yung, Y. L., Li, G. and Seinfeld, J. H.: Unexpected air pollution with marked emission reductions during the COVID-19 outbreak in China, Science (80-.)., 7431(June), eabb7431, doi:10.1126/science.abb7431, 2020.

Leighton, P. A.: Reactions of Ozone, in Photochemistry of Air Pollution, vol. 9, pp. 152–183, Elsevier., 1961.

Menut, L., Bessagnet, B., Siour, G., Mailler, S., Pennel, R. and Cholakian, A.: Impact of lockdown measures to combat Covid-19 on air quality over western Europe, Sci. Total Environ., 741, 140426, doi:10.1016/j.scitotenv.2020.140426, 2020.

Monks, P. S., Archibald, A. T., Colette, A., Cooper, O., Coyle, M., Derwent, R., Fowler, D., Granier, C., Law, K. S., Mills, G. E., Stevenson, D. S., Tarasova, O., Thouret, V., von Schneidemesser, E., Sommariva, R., Wild, O. and Williams, M. L.: Tropospheric ozone and its precursors from the urban to the global scale from air quality to short-lived climate forcer, Atmos. Chem. Phys., 15(15), 8889–8973, doi:10.5194/acp-15-8889-2015, 2015.

Ordóñez, C., Garrido-Perez, J. M. and García-Herrera, R.: Early spring near-surface ozone in Europe during the COVID-19 shutdown: Meteorological effects outweigh emission changes, Sci. Total Environ., 747(December 2019), 141322, doi:10.1016/j.scitotenv.2020.141322, 2020.

Petetin, H., Bowdalo, D., Soret, A., Guevara, M., Jorba, O., Serradell, K., and Pérez García-Pando, C.: Meteorology-normalized impact of the COVID-19 lockdown upon NO2 pollution in Spain, Atmos. Chem. Phys., 20, 11119–11141, https://doi.org/10.5194/acp-20-11119-2020, 2020.

Shi, X. and Brasseur, G. P.: The Response in Air Quality to the Reduction of Chinese Economic Activities During the COVID- 19 Outbreak, Geophys. Res. Lett., 47(11), e2020GL088070-e2020GL088070, doi:10.1029/2020GL088070, 2020.

Sicard, P., De Marco, A., Agathokleous, E., Feng, Z., Xu, X., Paoletti, E., Rodriguez, J. J. D. and Calatayud, V.: Amplified ozone pollution in cities during the COVID-19 lockdown, Sci. Total Environ., 735, 139542, doi:10.1016/j.scitotenv.2020.139542, 2020.

Venter, Z. S., Aunan, K., Chowdhury, S. and Lelieveld, J.: COVID-19 lockdowns cause global air pollution declines, Proc. Natl. Acad. Sci., 5(11), 202006853, doi:10.1073/pnas.2006853117, 2020.

Wang, Y. and Jacob, D. J.: Anthropogenic forcing on tropospheric ozone and OH since preindustrial times, J. Geophys. Res. Atmos., 103(D23), 31123–31135, doi:10.1029/1998JD100004, 1998.

Yan, Y., Lin, J., Pozzer, A., Kong, S. and Lelieveld, J.: Trend reversal from high-to-low and from rural-to-urban ozone concentrations over Europe, Atmos. Environ., 213(January), 25–36, doi:10.1016/j.atmosenv.2019.05.067, 2019.

Supporting information

***Table S1**. "Urban" stations. Anomalies of the mean concentration of CO, NO_2, SO_2, O_3 and PM_{10} in 2020 compared to the average of the previous seven years (2013-2019) for the period 18 March to 18 May, measured at 421 "urban" AirBase stations (defined as located in high-density areas with a population density greater than 1500 inhabitants/km2). The distribution of the anomalies for all stations is given by five percentiles (P10, P25, P50, P75, P90); "% avail." indicates the percentage of available stations. The upper part of the table presents the anomalies in terms of concentrations (in $\mu g.m^{-3}$), and the lower part in terms of relative change (in %) against the 7-year average.*

µg.m³	P10	P25	P50	P75	P90	% avail.
CO	-81.5	-53.3	-27.1	10.7	129.2	15
PM_{10}	-4.5	-2.9	-1.2	0.6	1.9	60
NO_2	-16.1	-11.4	-7.9	-5.3	-2.9	82
O_3	-4.0	1.9	6.8	10.6	13.5	68
SO_2	-1.9	-0.9	-0.3	0.2	0.9	27

%	P10	P25	P50	P75	P90	% avail.
CO	-30	-18	-10	3	38	15
PM_{10}	-24	-14	-6	3	10	60
NO_2	-58	-51	-40	-29	-19	82
O_3	-6	3	11	18	25	68
SO_2	-52	-37	-12	6	51	27

***Table S2**. "Rural" stations. Anomalies of the mean concentration of CO, NO_2, SO_2, O_3 and PM_{10} in 2020 compared to the average of the previous seven years (2013-2019) for the period 18 March to 18 May, measured at 887 "rural" AirBase stations (defined as located in low-density areas with a population density lower than 1500 inhabitants/km2). The distribution of the anomalies for all stations is given by five percentiles (P10, P25, P50, P75, P90); "% avail." indicates the percentage of available stations. The upper part of the table presents the anomalies in terms of concentrations (in $\mu g.m^{-3}$), and the lower part in terms of relative change (in %) against the 7-year average.*

µg.m³	***P10***	***P25***	***P50***	***P75***	***P90***	*% avail.*
CO	-85.7	634.6	1.2	96.9	243.8	*10*
PM_{10}	-4.0	-2.4	-0.6	1.3	3.4	*50*
NO_2	-9.6	-6.6	-3.9	-1.9	-0.7	*67*
O_3	-12.0	-4.1	3.1	7.6	10.6	*68*
SO_2	-1.9	-0.8	-0.1	0.2	1.1	*27*

%	***P10***	***P25***	***P50***	***P75***	***P90***	*% avail.*
CO	-30	-14	1	32	123	10
PM_{10}	-21	-13	-3	7	20	50
NO_2	-60	-49	-35	-23	-12	67
O_3	-15	-6	5	12	18	68
SO_2	-56	-35	-10	17	60	27

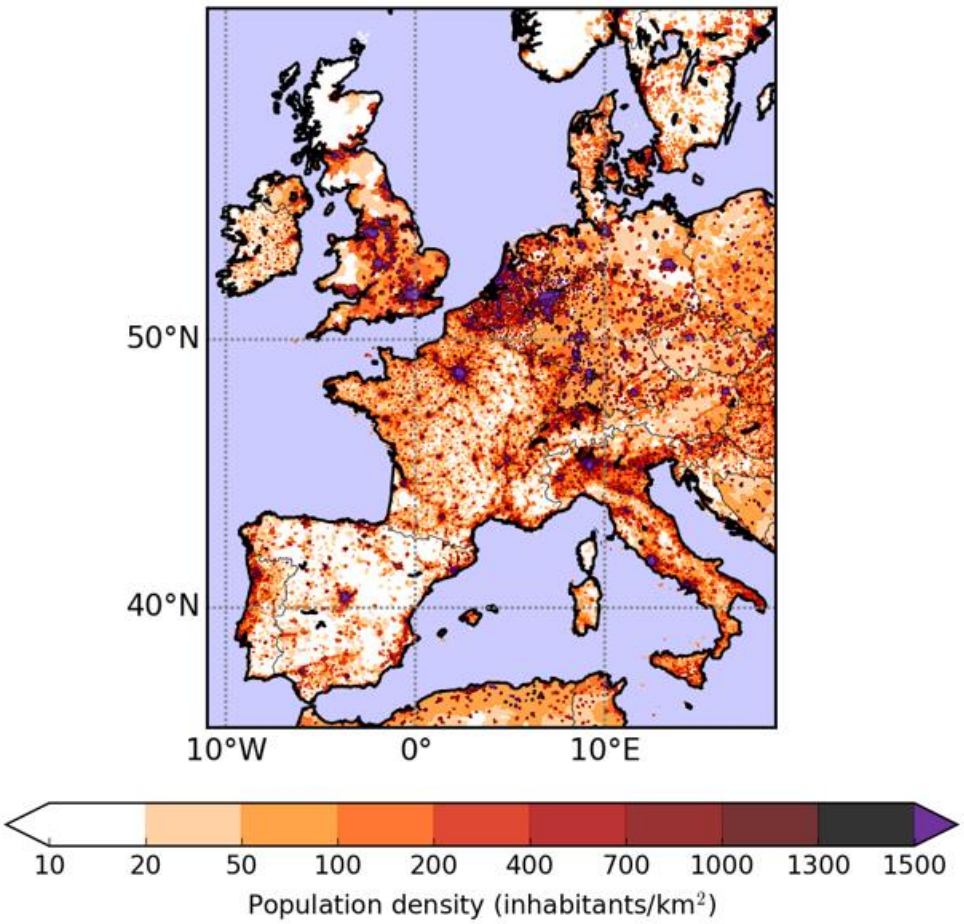

***Figure S1**. Population density in Europe (data from NASA/SEDAC 2005).*

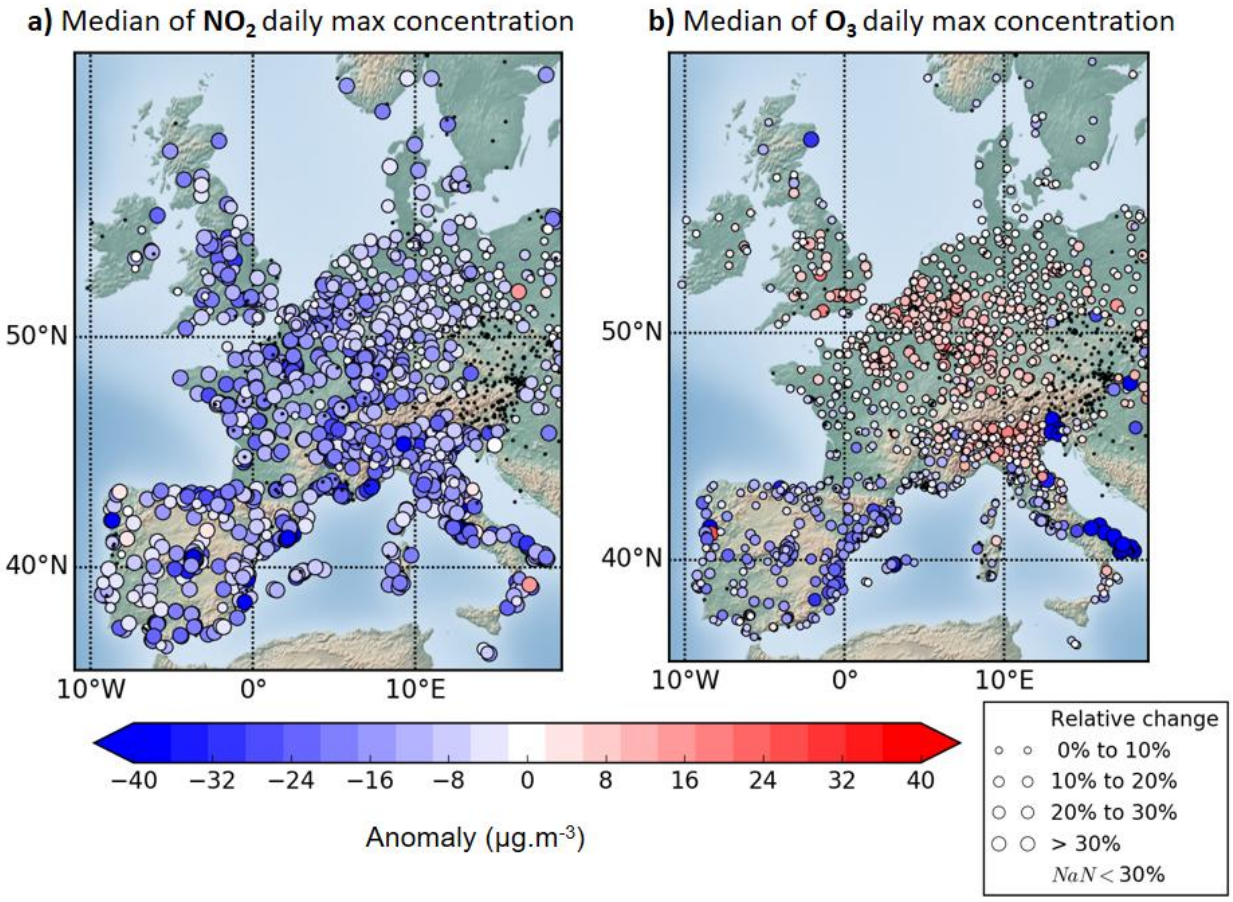

***Figure S2**. Anomalies of **(a)** NO_2 and **(b)** O_3 medians of daily maximum concentration at AirBase stations in 2020 compared to the previous seven years (2013-2019) for the period 18 March to 18 May. The dots are colored according to the anomalies in concentration (in µg.m^{-3}) and sized proportionally to the relative change (in %). The black dots correspond to stations with less than 30% of available data.*

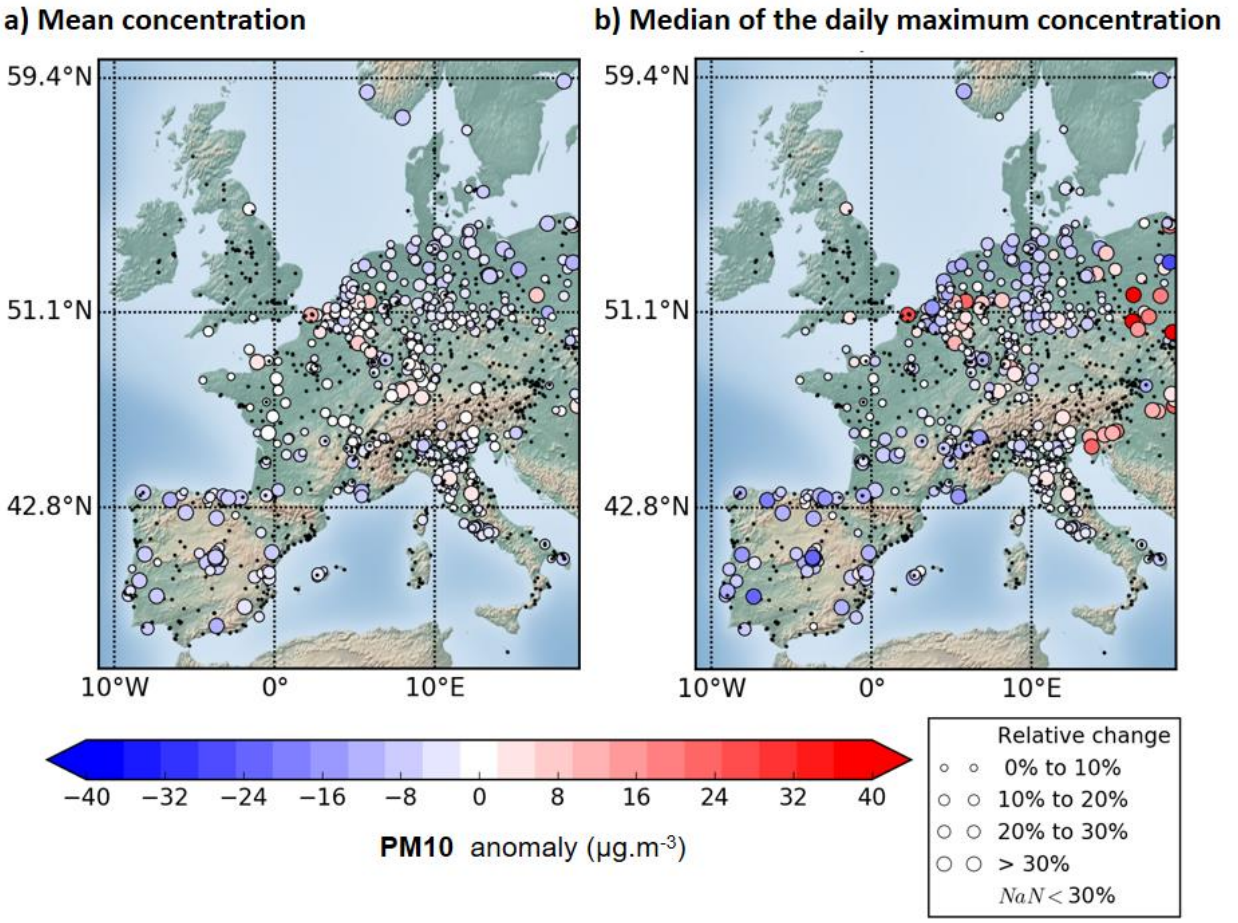

***Figure S3**. Anomalies of the PM_{10} concentration at AirBase stations in 2020 compared to the previous seven years (2013-2019) for the period 18 March to 18 May. The dots are colored according to concentration (in $\mu g.m^{-3}$) and sized proportionally to the relative change (in %). **(a)** Anomalies of mean PM_{10} concentrations. **(b)** Anomalies of the median of daily maximum PM_{10} concentrations. The black dots correspond to stations with less than 30% of available data.*

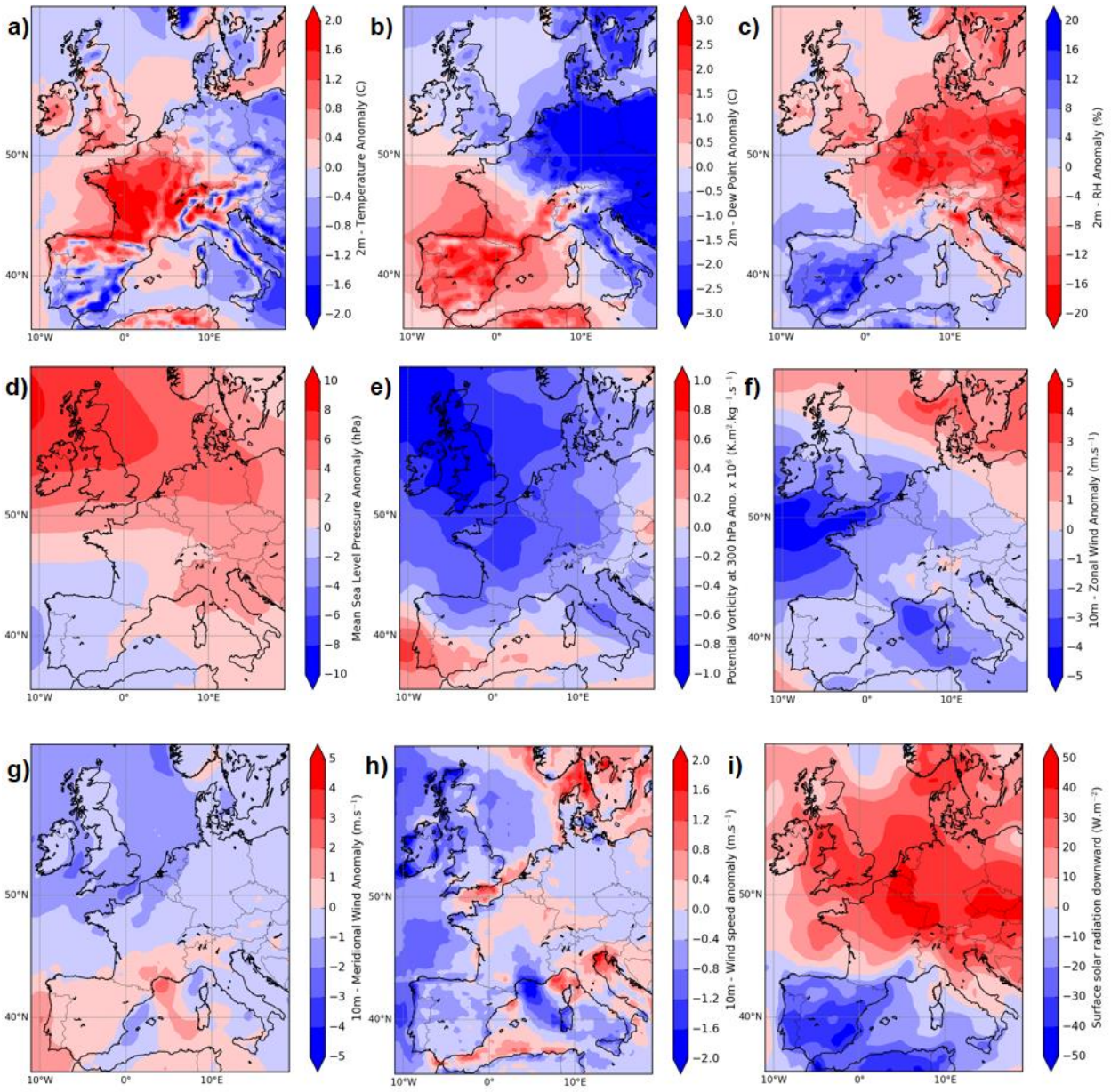

Figure S4*. Meteorological anomalies of 2020 compared to a 7-year (2013-2019) average for the period 18 March to 18 May using data at 0.125°x0.125° resolution from the ECMWF-IFS model of: (a) 2m-temperature, (b) 2m-dew point, (c) 2m-relative humidity, (d) mean sea level pressure, (e) potential vorticity at 300 hPa, (f) 10m-zonal wind, (g) 10m-meridional wind, (h) 10m-wind speed, and (i) surface solar radiation downward****.***

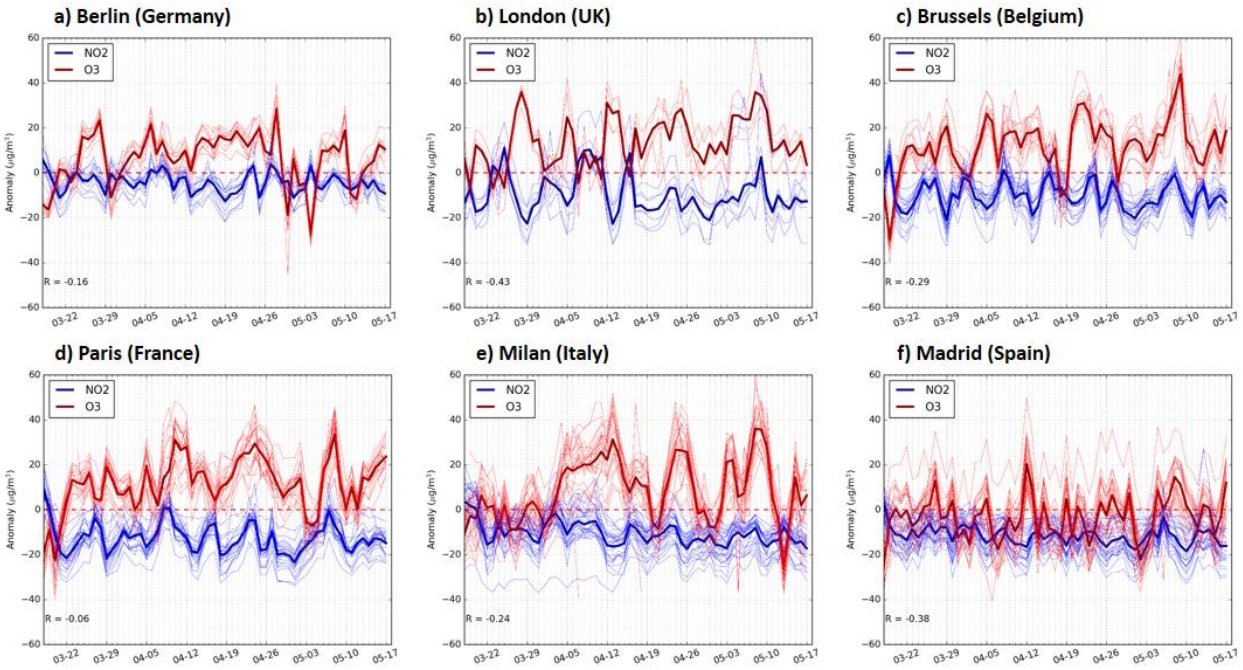

Figure S5. *Daily mean concentrations of NO_2 (blue lines) and O_3 (red lines) of each monitoring station and of the average of all stations (bold lines) at six major European cities: (a) Berlin (Germany), (b) London (UK), (c) Brussels (Belgium), (d) Paris (France), (e) Milan (Italy) and (f) Madrid (Spain).*